East African Journal of Engineering
eaje.eanso.org
Volume 7, Issue 1, 2024
Print ISSN: 2707-5389 | Online ISSN: 2707-5397
Title DOI: https://doi.org/10.37284/2707-5397

EAST AFRICAN NATURE & SCIENCE ORGANIZATION

Original Article

Comparative Analysis of Performance of Mat Foundations in Non-liquefiable and Liquefiable Soil

Tukashaba Shafan[1*] *& Ping Yi*[1]

[1] Dalian University of Technology, Dalian 116024, Liaoning.
* Author for Correspondence ORCID ID: https://orcid.org/0009-0002-1265-475X; Email: shafantukashaba@gmail.com

Article DOI : https://doi.org/10.37284/eaje.7.1.1991

Publication Date:

13 June 2024

Keywords:

Foundation Engineering, Soil Liquefaction, Mat Foundations, Bearing Capacity, Design Optimization

ABSTRACT

This study investigates the behaviour and performance of mat foundations in non-liquefiable and liquefiable soil, aiming to provide insights for engineers under soil liquefaction conditions. Through finite element analyses, the study explores shallow foundation design complexities, assesses the bearing capacities of mat foundations under liquefaction soil characteristics, and offers data-driven design strategies for such conditions. The findings on mat foundations in liquefiable soil reveal that iterative dimension adjustments lead to significant enhancements in bearing capacity, hence exceeding the load-bearing capacity in non-liquefiable soil that is used as benchmark. The modification factors range from 2.4 to 2.6 times the original dimensions verified to be effective. These results emphasize the role of tailored design adjustments and numerical designs in solving diverse soil settings and enhancing structural safety, performance, and integrity in foundation design, especially in challenging soil conditions with liquefaction.

APA CITATION

Shafan T. & Yi P. (2024). Comparative Analysis of Performance of Mat Foundations in Non-liquefiable and Liquefiable Soil *East African Journal of Engineering*, 7(1), 187-198. https://doi.org/10.37284/eaje.7.1.1991

CHICAGO CITATION

Shafan, Tukashaba and Ping Yi. 2024. "Comparative Analysis of Performance of Mat Foundations in Non-liquefiable and Liquefiable Soil". *East African Journal of Engineering* 7 (1), 187-198. https://doi.org/10.37284/eaje.7.1.1991.

HARVARD CITATION

Shafan T. & Yi P. (2024) "Comparative Analysis of Performance of Mat Foundations in Non-liquefiable and Liquefiable Soil", *East African Journal of Engineering*, 7(1), pp. 187-198. doi: 10.37284/eaje.7.1.1991.

IEEE CITATION

T., Shafan & P., Yi "Comparative Analysis of Performance of Mat Foundations in Non-liquefiable and Liquefiable Soil" *EAJE*, vol. 7, no. 1, pp 187-198, Jun. 2024.

MLA CITATION

Shafan, Tukashaba & Ping Yi. "Comparative Analysis of Performance of Mat Foundations in Non-liquefiable and Liquefiable Soil" *East African Journal of Engineering*, Vol. 7, no. 1, Jun. 2024, pp. 187-198, doi:10.37284/eaje.7.1.1991.

INTRODUCTION

In foundation engineering, Terzaghi's bearing capacity equation, developed in 1943, stands as a cornerstone for evaluating the load-bearing capacity of shallow foundations, such as mat foundations (MF) facing general shear failure (Coduto, 2015; Bahloul et al., 2004). This equation takes into account critical parameters such as cohesion (c'), overburden pressure (q), unit weight of soil (γ), and foundation width (B), along with dimensionless bearing capacity factors (N_c, N_q, and N_γ) derived from the effective internal angle of friction (φ'). Terzaghi's analysis, rooted

Article DOI: https://doi.org/10.37284/eaje.7.1.1991

in limit equilibrium principles, envisions the foundation's bearing capacity (BC) as the pressure threshold where the triangular zone beneath the footing is poised for downward motion, with radial shear zones shifting laterally and Rankine passive zones uplifting (Kang and Jie, 2017).

Figure 1: Mat foundation

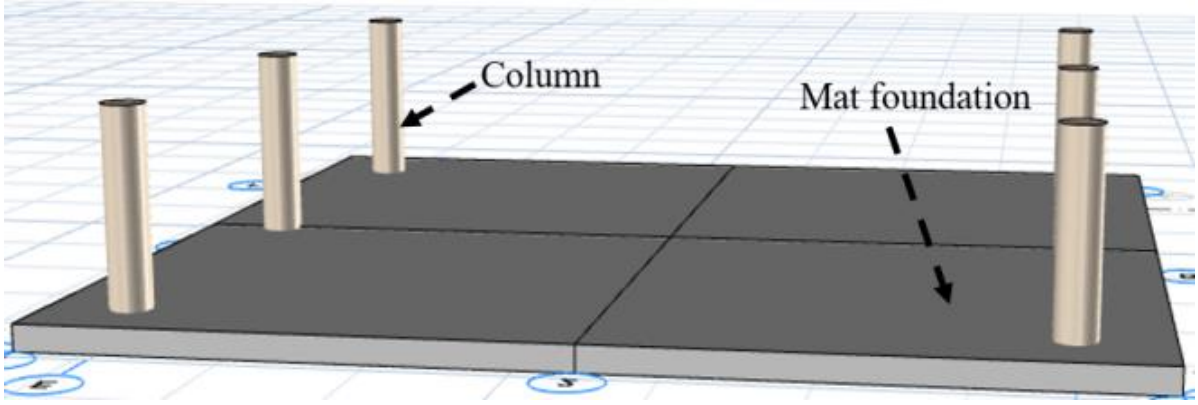

The ultimate bearing capacity (q_u) signifies the maximum load soil can endure, while the allowable bearing capacity (q_{all}) is derived by dividing the gross ultimate bearing capacity ($q_{u,gross}$) obtained from Terzaghi's equation by a factor of safety equal to or exceeding 3 (Terzaghi, 1943). Practical engineering applications further refine this concept into the net allowable bearing capacity ($q_{all(net)}$), considering the actual applied stress from the structure to provide a more precise representation of the soil's bearing capacity.

In regions susceptible to liquefaction, where the stability and integrity of foundations are at heightened risk, the study of mat foundations in liquefiable soils becomes crucial. The primary objectives of this research are twofold: first, to evaluate and compare the bearing capacity of mat foundations under various conditions associated with soil liquefaction; and second, to provide engineers with data-driven design strategies for foundations in liquefaction-prone areas. Through iterative simulations and analyses, the research aims to determine optimal dimensions and design modifications for mat foundations, enabling them to withstand the challenges posed by soil liquefaction while maintaining stability, strength, and safety at an economic cost (Jelušič & Žlender, 2018).

Despite extensive research on the bearing capacity of mat foundations, several critical gaps persist, especially regarding their performance in liquefaction-prone regions. Previous studies have predominantly focused on general shear failure scenarios, often neglecting the complex behavior of mat foundations during soil liquefaction events (Siragy, 2019). There is a pressing need for detailed investigations into how liquefaction impacts bearing capacity and foundation stability. Additionally, much of the existing research assumes homogeneity in soil properties, whereas actual conditions can vary significantly, particularly in liquefiable areas (Helwany, 2007). A nuanced understanding of these variations is essential for accurate assessment of foundation performance (Coduto, 2015).

Moreover, many studies rely on simplified models that do not fully capture the dynamic nature of soil-structure interactions during seismic events (McGann et al., 2012). Advanced simulations incorporating realistic loading conditions and soil behavior under liquefaction are needed to enhance design accuracy. Furthermore, specific guidelines and strategies tailored to the unique challenges of designing mat foundations for liquefiable soils are sparse, leaving engineers without the targeted data and recommendations critical for ensuring safety and efficacy (Fan et al., 2017).

Finally, there is a notable gap in research aimed at balancing safety and economic efficiency in foundation design for liquefaction-prone areas. Identifying cost-effective design modifications and optimal foundation dimensions that ensure

Article DOI: https://doi.org/10.37284/eaje.7.1.1991

structural integrity without excessive costs is crucial (Jelušič & Žlender, 2018). Addressing these gaps will improve the reliability and cost-effectiveness of mat foundation designs in liquefaction-prone regions, ensuring both safety and economic viability in engineering practice.

METHODOLOGY

Table 1 provides foundation soil parameters from two studies: (Kang & Jie, 2017) and (Rostami et al., 2017) and were utilized in the finite element analyses. For non-liquefiable soil, parameters are derived from both studies, whereas liquefiable soil parameters are based solely on Rostami et al. (2017). Note that all these soil properties have different parameters, for instance, the non-liquefiable soil (NLS) layer of medium-dense silty sand (MDSS) is different from the liquefiable soil (LS) layer of MDSS. Key parameters relevant to liquefaction susceptibility include cohesion, friction angle, and Young's modulus. Liquefaction occurs more readily in soils with lower cohesion and friction angles, and lower values of Young's modulus indicate greater compressibility, increasing vulnerability to liquefaction. The liquefiable soil exhibits a lower Young's modulus and a slightly lower friction angle compared to non-liquefiable soils, as shown in *Table 1*, indicating a higher susceptibility to liquefaction-induced deformations and damage.

Modeling the Soil

In this study, a distinct 3D model of soil configuration surrounding the footing was examined, with a homogenous thickness of the liquefied layer as well as material properties, to investigate how a footing performs in liquefaction events. Soil parameters, drawn from previous case studies (Rostami et al., 2017; Sarkar et al., 2014), were meticulously chosen to ensure the validity of the results. During liquefaction events, the pore water pressure within the liquefiable layer increases, resulting in a reduction of effective stress and a consequent decrease in shear strength. This phenomenon significantly affects the compressibility of the layer. Therefore, soil material parameters were chosen with the assumption that the bulk modulus K remains consistent throughout the soil mass, while a Poisson's ratio of 0.485 was selected for liquefiable soils (Rostami et al., 2017; McGann et al., 2012). Moreover, the behaviour of soils was simulated using the Mohr–Coulomb failure criterion (Helwany, 2007).

Boundary Condition

When simulating how foundations interact with soil using the FEA, getting the boundary conditions right is really important. This is especially true when looking at dynamic load scenarios, where the conditions need to keep the elements in place while preventing them from moving too much. For example, in this research that compared FEA with Terzaghi's solution, a three-dimensional model was used that had fixed base boundaries and vertically constrained horizontal boundaries. The model used linear brick elements with reduced integration (C3D8R) and had a finer mesh around the foundation to accurately capture stress concentration areas.

The loading was applied gradually at a constant downward velocity (v = 6 cm/s) boundary conditions to prevent the model from becoming excited. These specific boundary conditions not only allow for more realistic simulations but also make it easier to compare the results with existing solutions, such as Terzaghi's equation. The concept of finer mesh is further elucidated in *Figure 2b*.

Mat Foundation In Non-Liquefiable Soil with Length, L = 1.5m and width, B = 1.5m (Ottawa sand)

Using Terzaghi's equation, calculate the bearing capacity of a 1.5 m × 1.5 m foundation on a homogeneous layer of Ottawa sand (c' = 0 and φ' = 30°). The foundation is situated at a depth D_f = 0.5 m. The unit weight of soil is 18 kN/m^3 as shown in *Table 1*.

Solve part (a) using the finite element method. Assume that Ottawa sand has the properties described in *Table 1*. Use both the Mohr-Coulomb (MC) and the cap model to simulate sand behavior. Compare the finite element prediction

Article DOI: https://doi.org/10.37284/eaje.7.1.1991

of bearing capacity with that predicted by Terzaghi's equation.

Finite element solution: the analysis employs the cap model, a modification of the Drucker–Prager (DP) model with a cap, which is calibrated to match the parameters of the classical Mohr-Coulomb yield model, namely cohesion (c') and friction angle (φ'). The geometric setup, boundary conditions, and material properties mirror those outlined in part (a), facilitating a direct comparison between the finite element analysis outcomes and Terzaghi's solution.

Table 1: Soil properties for non-liquefiable and liquefiable soils

Type	Basic description	Unit weight (kN/m^3)	Cohesion, c' (kPa)	Friction angle, φ' ($^\circ$)	Young's modulus, E (kPa)	Poisson Ratio, v	Shear modulus, G (kPa)	Bulk modulus, K (kPa)
NLS	Ottawa sand	18.0	0.0	30.0	30000	0.3	11538.5	25000
NLS	MDSS	18.0	0.0	32.0	25000	0.35	9260	27777.8
LS	MDSS	18.0	0.0	30.0	2500	0.485	842	27777.8

Source: (Kang and Jie, 2017)

The three-dimensional model depicted in *Figure 2a* encompasses a sand layer measuring 50 meters deep and 100 meters by 100 meters in plan. The loaded area occupies a space of 1.5 meters by 1.5 meters. This loaded area emulates a foundation with ideal contact with the soil. Linear brick elements with eight nodes and reduced integration are employed for the sand layer. The sand layer's base is fully fixed in all directions, while vertical boundaries are constrained horizontally but free vertically. *Figure 2b* displays the finite element mesh utilized in the analysis, with a finer mesh surrounding the foundation to capture stress concentration zones. The problem's geometry and boundaries were initially represented through mesh generation. Subsequent analysis and error estimation followed. A refinement strategy, either uniform or adaptive, was then selected to enhance the mesh in key areas. The solution was recalculated using the refined mesh, and convergence was assessed through result comparisons. Convergence criteria, aiming for diminishing changes with further refinement, were established based on observed trends. Adaptive refinement proved superior, particularly in regions with high gradients or complex phenomena, and thus adopted for all simulations. The entire process, including mesh, strategy, criteria, and findings, was thoroughly documented.

To facilitate comparison with Terzaghi's equation, the 0.5-meter-thick soil layer (referred to as the foundation depth, D_f) is substituted with an overburden pressure represented by $q = \gamma D_f = 18 \times 0.5 = 9$ kPa. This approach excludes the consideration of shear resistance from the 0.5-meter-thick soil layer in the finite element analysis, aligning with one of Terzaghi's assumptions for deriving his equation. The elastic behaviour of Ottawa sand is assumed to be linear and isotropic, characterized by Young's modulus of 30 MPa and a Poisson ratio of 0.3. Young's modulus is determined from the initial slope of the stress-strain triaxial test results (Helwany, 2007). Soil strength parameters $\varphi' = 30°$ and $c' = 0$ MPa are derived from the slope and intercept of the Mohr-Coulomb failure criterion.

In this instance, the parameters of a linear Drucker–Prager model, denoted as β and d, are adjusted to align with the Mohr-Coulomb parameters, namely φ' and c', under triaxial stress conditions, which are suitable for the stress conditions encountered in this three-dimensional problem. When dealing with triaxial stress conditions, the Mohr-Coulomb parameters ($\varphi' = 30°$ and $c' = 0$ MPa) can be converted to Drucker–Prager parameters using the following method:

$$\tan\beta = \frac{6\sin\varphi'}{3-\sin\varphi'} \quad \text{for } \varphi' = 30°, \ \rightarrow \beta = 50.2°$$

$$d = \frac{18c'\cos\varphi'}{3-\sin\varphi'} \quad \text{for } c' = 0, \ \rightarrow d = 0$$

Article DOI: https://doi.org/10.37284/eaje.7.1.1991

Figure 2: Idealization of the 3D mat foundation problem; and finite element discretization of the mat foundation problem

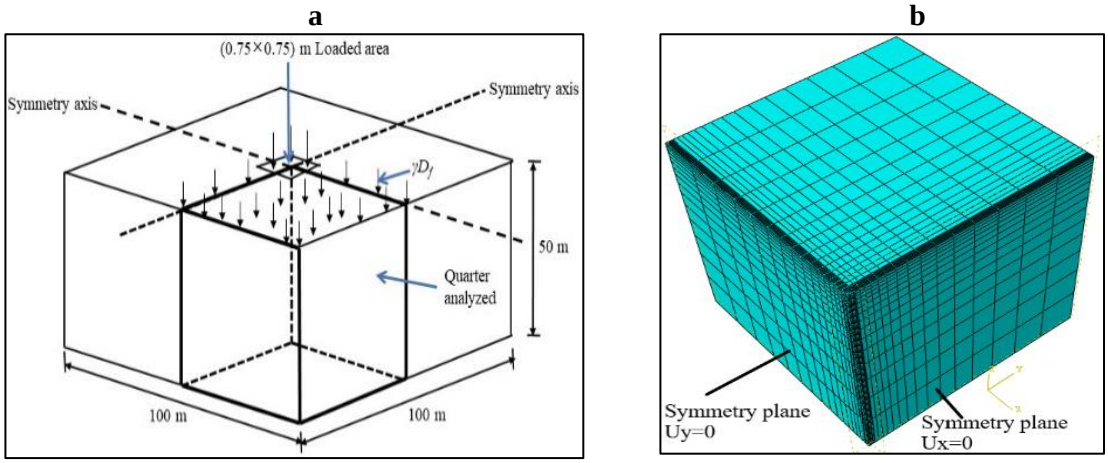

The cap eccentricity parameter is set at R = 0.4. The initial cap position, which reflects the initial consolidation of the specimen, is defined as $\varepsilon_{vol(0)}^{pl} = 0.0$, while the cap hardening curve is from an isotropic consolidation test conducted on Ottawa sand. The transition surface parameter α is determined to be 0.05. These parameters, outlined in *Table 2*, were employed to replicate the stress-strain curves of Ottawa sand under confining pressure.

Table 2: Cap model parameters for Ottawa sand

Density, ρ (kg/m^3)	Initial void ratio, e_0	β (°)	d	R	Initial yield	void ratio	K	α	E (MPa)	v	$\varepsilon_{vol(0)}^{pl}$
1800	1.5	50.2 (3-D)	10^{-5}	0.4	0.0	0.4-0.45	1	0.05	30	0.3	0.0

Table 3: Mat foundation's FEA and Terzaghi results (initial L and B = 1.5m)

Type	BC of MF [Terzaghi] (kPa)	Stress (kPa) (MC)	Stress (kPa) (cap model)	Force (kN) (MC)	Force (kN) (cap model)	q_{all} (kPa) [MC]
Non-liquefied sand (Ottawa sand)	367.42	2322.44	1880.71	5225.5	4231.59	774.15

In this example, we establish the load-displacement relationship for the 1.5 m × 1.5 m footing. The bearing capacity of the footing can be determined from the load-displacement curve. Dynamic-explicit analysis was employed, and the loading was applied very gradually to prevent exciting the model. It's worth noting that explicit analyses automatically utilize very small-time increments to ensure stability, which can result in increased computational expense.

At the outset of the analysis, gravity loads and surcharge loads are imposed on the sand layer, playing a crucial role in establishing the initial stresses within all soil elements. Given the stress-dependent nature of soil behaviour, it's essential to consider these loads. The cap model employed in this study acknowledges this key aspect. In this analysis, the foundation load was applied via a constant downward velocity boundary condition at the top surface of the foundation, with a velocity (v) set at 6 cm/s over a duration of 10 seconds.

Figure 3a displays the pressure–settlement curves for dynamic–explicit analysis. For comparison, the bearing capacity of 367 kPa predicted by Terzaghi's equation (part a) is also depicted in

Article DOI: https://doi.org/10.37284/eaje.7.1.1991

Figure 3a and the force carried by the mat foundation is shown in *Figure 3b* Approximately the bearing capacities of 5225.5 kN (MC) and 4231.59 kN (cap model) are predicted. It's worth noting that the finite element prediction of bearing capacity slightly exceeds Terzaghi's bearing capacity.

Figure 3: Load-displacement curve: comparison of FEA results with Terzaghi calculation; and force carried by mat foundation in non-liquefied sand

a **b**

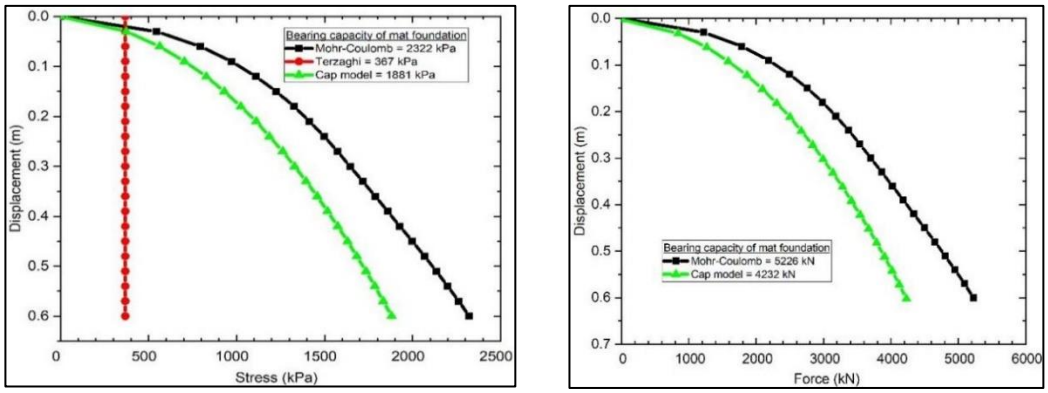

Several factors contribute to this difference, with the primary one being the underlying assumptions of Terzaghi's equation compared to the finite element analysis (Terzaghi, 1943; Terzaghi et al., 1996). Terzaghi's equation assumes the soil behaves as a rigid–perfectly plastic material, experiencing abrupt failure once the bearing capacity is reached. In contrast, the finite element analysis considers the soil as an elastoplastic material with hardening behaviour (Helwany, 2007; Zienkiewicz et al., 2005). Such a material undergoes deformation under applied loads, unlike a rigid material. Additionally, the finite element formulation allows for progressive yielding, where elements can yield gradually and progressively. As one element yields, it can influence neighboring elements to yield as well, leading to a progressive development of shear surfaces akin to the one depicted in *Figure 4a*.

Figure 4: Plastic shear strain distribution at failure; vertical stress distribution at failure; stress concentration in the soil; and deformation of the soil model

a **b**

c **d**

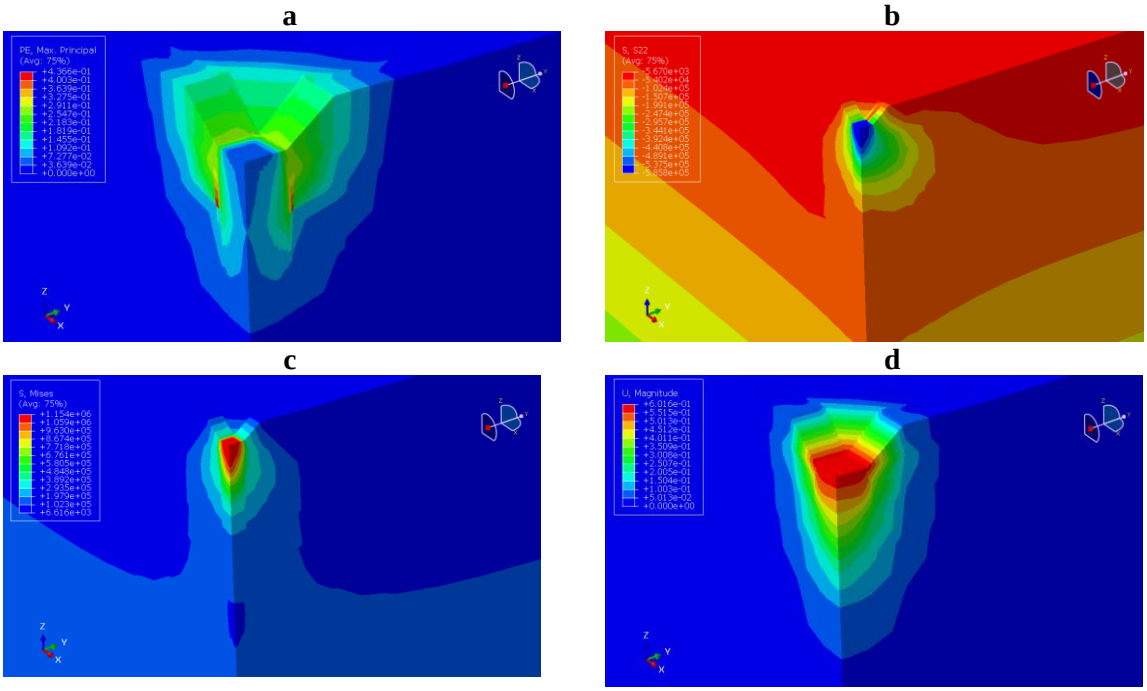

Article DOI: https://doi.org/10.37284/eaje.7.1.1991

Figure 4a displays the contours of plastic shear strain in the sand layer at the point of failure load, while *Figure 4b* illustrates the contours of vertical stresses in the sand layer at the failure load. *Figure 4c* and *d* show stress concentration and deformation of the soil model.

Mat Foundation in Non-Liquefiable soil with *L* = 1.5m and *B* = 1.5m (MDSS)

- Determine the bearing capacity of a 1.5 m x 1.5 m foundation on a homogeneous layer of NLS MDSS sand (c' = 0 and φ' = 32°) using Terzaghi's equation. The depth of the footing is D_f = 0.5 m. The soil's unit weight is 18 kN/m^3, with other values as indicated.
- Apply the FE technique to solve component (a). Assume that the characteristics listed in *Table 1* apply to NLS MDSS. Utilize the Mohr-Coulomb model to model the behavior of sand. Compare the bearing capacity predicted by Terzaghi's equation with the finite element prediction.

Note: In the previous example, we utilized both the Mohr-Coulomb (MC) model and the cap model. However, to expedite proceedings, the study will exclusively employ the MC model for all subsequent examples and analyses.

Table 4: Mat foundation results (initial *L* and *B* = 1.5m)

Type	BC of MF (kPa) [Terzaghi]	Stress (kPa) [MC]	Force (kN) [MC]	q_{all} (kPa) [MC]
NLS (MDSS)	488.84	2507.44	5641.73	835.81

Figure 5: Load-displacement curve: contrasting the Terzaghi computation with the FEM results; force carried by the mat foundation in non-liquefied sand; distribution of plastic shear strain at failure; vertical stress distribution at failure; stress concentration

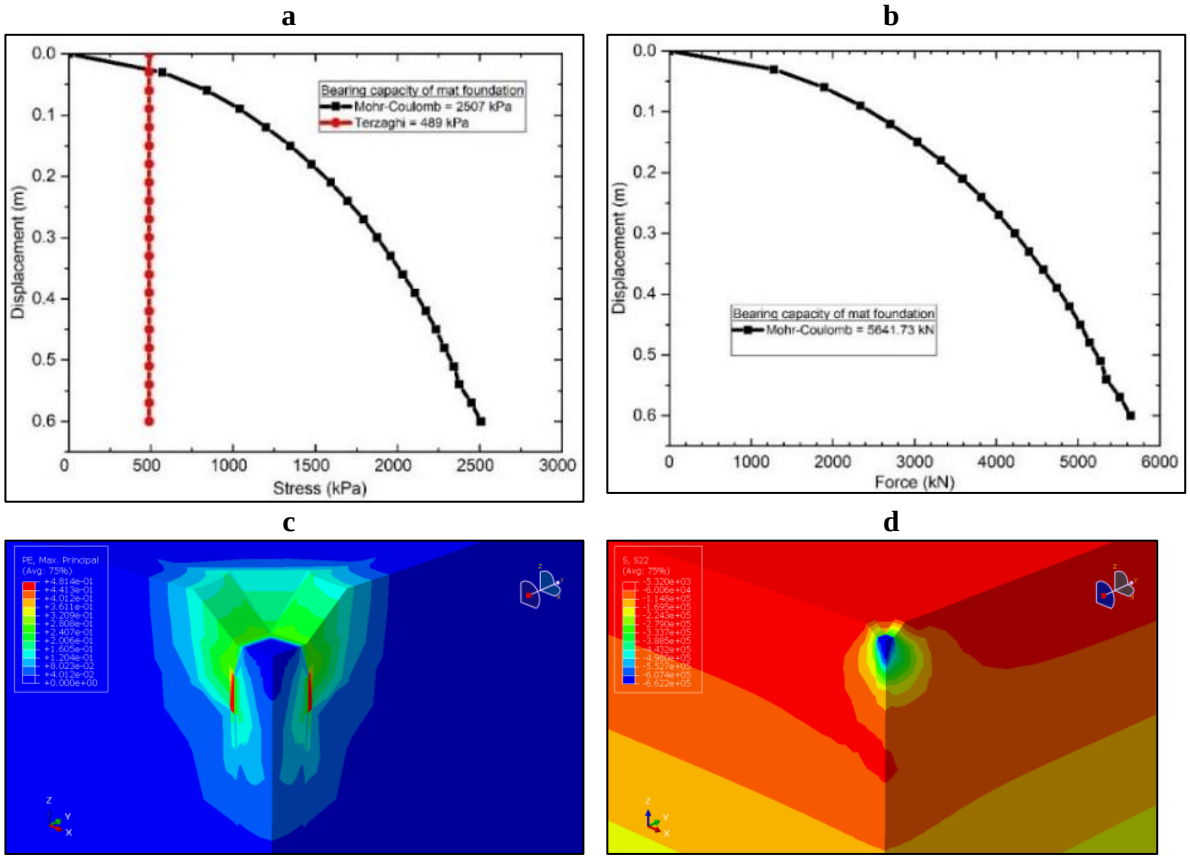

Article DOI: https://doi.org/10.37284/eaje.7.1.1991

e

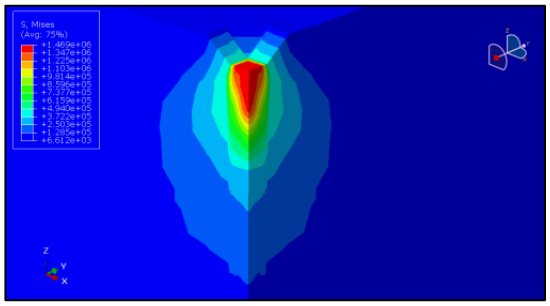

f

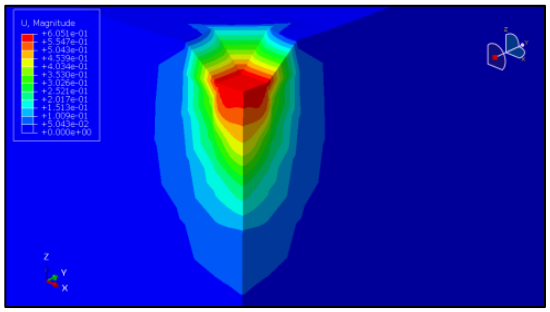

Mat foundation in liquefiable soil with length, *L* = 1.5m and width, *B* = 1.5m (MDSS)

- Using Terzaghi's equation, calculate the bearing capacity of a 1.5 m × 1.5 m foundation on a homogeneous layer of MDSS (c' = 0 and φ' = 30°). The foundation is situated at a depth D_f = 0.5 m. The unit weight of soil is 18 kN/m^3.
- Solve part (a) using the finite element method. The liquefiable soil is a medium-dense silty sand and has the properties described in *Table 1*. Use the Mohr-Coulomb model to simulate sand behaviour. Compare the finite element prediction of bearing capacity with that predicted by Terzaghi's equation.

Table 5 Mat foundation results (initial *L* and *B* = 1.5m)

Type	Basic description	BC (kPa) [Terzaghi]	Stress (kPa) [MC]	Force (kN) [MC]	q_{all} (kPa) [MC]
Liquefied sand	Medium dense silty sand	367.42	713.6	1605.59	237.87

Figure 6: Load-displacement curve: comparison of FEA results with Terzaghi calculation; force carried by the mat foundation; plastic shear strain distribution at failure; vertical stress distribution at failure; stress concentration in the soil; and deformation

a

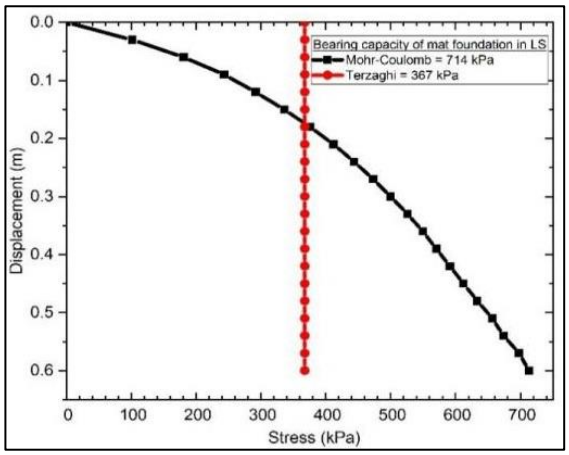

b

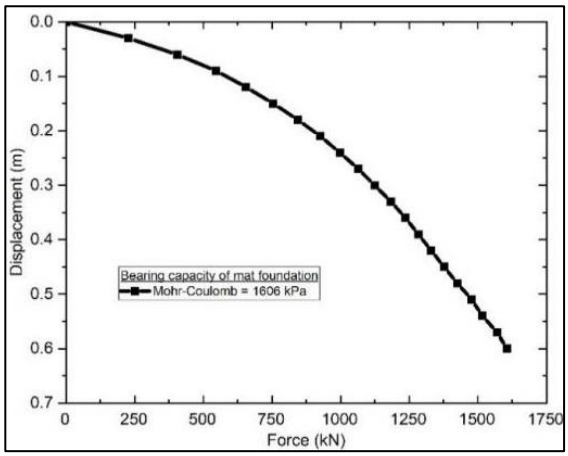

c

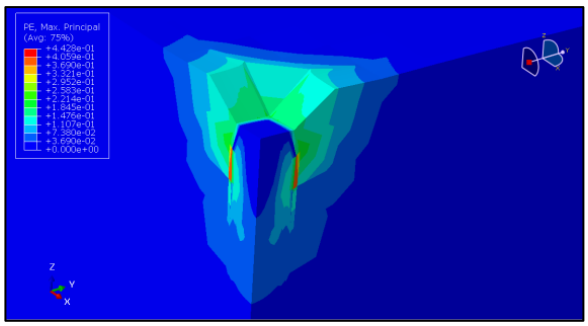

d

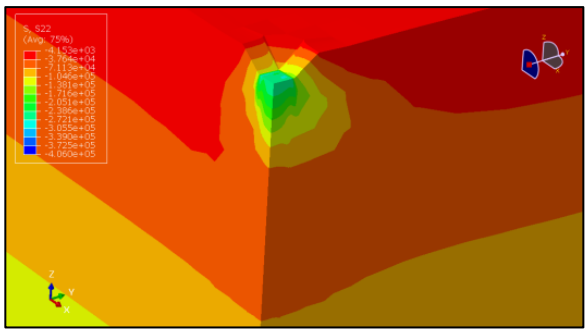

Article DOI: https://doi.org/10.37284/eaje.7.1.1991

e **f**

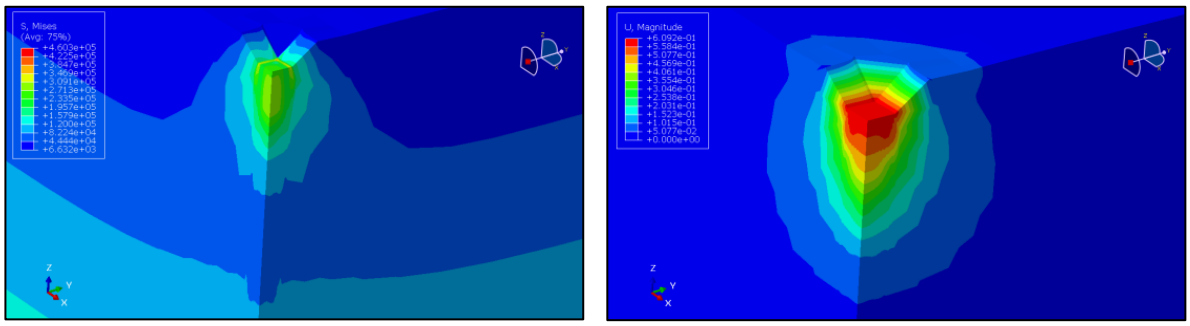

FINDINGS AND DISCUSSION

In the discussion of mat foundations, we conducted simulations to evaluate their performance in both liquefiable and non-liquefiable soils. Initially, the bearing capacity of mat foundations in non-liquefiable soil ranged from 5225.5 kN to 5641.73 kN, setting the benchmark for comparison as shown in *Table 6.*

Table 6 Modified mat foundation results (initial *L* and *B* = 1.5m)

Type	Description	Mod factor	*L*' & *B*' (m)	BC of MF (kPa) [Terzaghi]	Stress (kPa) [MC]	Force (kN) [MC]	q_{all} (kPa) [MC]
NLS	Ottawa sand	-	1.5	367.42	2322.44	5225.5	774.15
NLS	MDSS	-	1.5	488.84	2507.44	5641.73	835.81
LS	MDSS	-	1.5	367.42	713.6	1605.59	237.87
		2.0	3.0	532.71	470.1	4230.94	156.7
		2.33	3.5	587.80	442.3	5418.19	147.43
		2.4	3.6	598.82	440.2	5705.02	146.73
		2.5	3.75	615.35	411.38	5785.1	137.13

To ensure that mat foundations (for the first type of mat foundation that had an initial *L* and *B* of 1.5m) in liquefiable soil could withstand comparable loads, we increased their dimensions by 2.0 and 2.33 times, resulting in modified foundations capable of bearing forces of 4230.94 kN and 5418.19 kN, respectively. However, these capacities fell short of the targets observed in non-liquefiable soil.

Subsequent iterations involved further dimension adjustments, progressively increasing the dimensions by factors ranging from 2.4 to 2.5 times. These modifications led to significant enhancements in bearing capacity (as shown in *Figure 7*), with the final iterations achieving capacities exceeding those observed in non-liquefiable soil. Notably, the foundation with initial *L* and *B* of 1.5m dimensions was extended by up to 2.4 times, resulting in bearing capacities surpassing the highest observed capacity in non-liquefiable soil, thus fulfilling the desired objectives as shown in *Table 6*.

For another type of mat foundation that had an initial *L* and *B* of 15m, dimensions were increased by up to 2.6 times, resulting in bearing capacity (194429 kN) surpassing the highest observed capacity in non-liquefiable soil (191801 kN) as shown in *Table 7*, thus fulfilling the desired objectives.

Additionally, it is important to note that while these modifications yielded substantial improvements in bearing capacity, designing for the worst-case scenario remains advisable to ensure structural integrity and safety (Bahloul et al., 2004; Coduto, 2015; Zhang et al., 2021).

In summary, through iterative simulations and dimension adjustments, mat foundations in liquefiable soil were successfully optimized to withstand forces equivalent to or greater than those observed in non-liquefiable soil conditions,

Article DOI: https://doi.org/10.37284/eaje.7.1.1991

highlighting the effectiveness of tailored design approaches in addressing the challenges posed by soil liquefaction.

Table 7 Modified mat foundation results (initial *L* and *B* = 15m)

Type	Description	Mod factor	*L'* & *B'* (m)	Stress (kPa) [MC]	Force (kN) [MC]	q_{all} (kPa) [MC]
NLS	Ottawa sand	-	15	827.01	186078	275.67
NLS	MDSS	-	15	852.45	191801	284.15
LS	MDSS	-	15	187.20	42120	62.4
		2.567	38.5	127.78	189399	42.59
		2.6	39	127.83	194429	42.61
		2.67	40	127.83	204522	42.61

Figure 7: Force carried by mat foundation in both liquefiable and non-liquefiable soil

a **b**

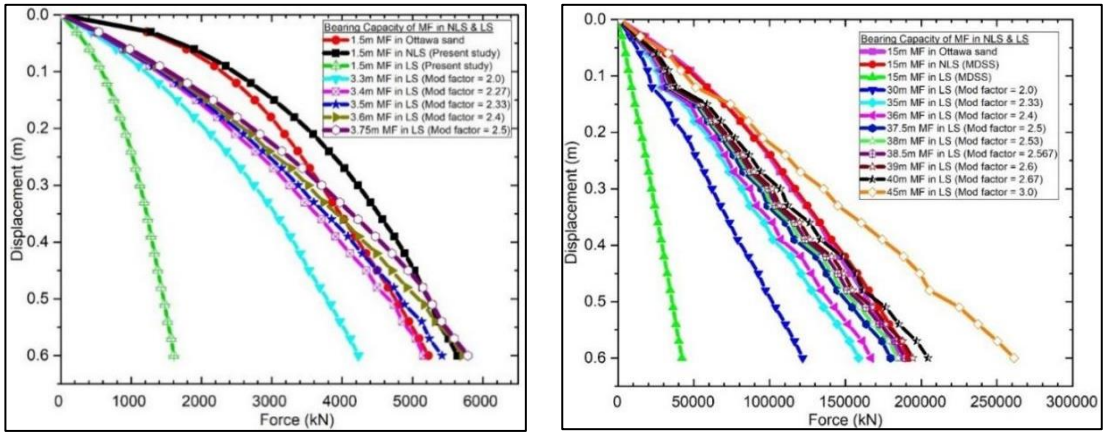

Failure Mode Identification

Figure 8 elucidates the anticipated failure mode, suggesting that as the mat footing size increases, the failure mode undergoes a significant shift toward punching shear failure. In essence, larger footings fail predominantly in punching shear. This is expected, considering that the relative compressibility of soils tends to increase with footing size.

Punching shear failure is a phenomenon typically observed in fairly loose soil conditions, characterized by a lack of distinct shear surfaces associated with general shear failure. In this failure mode, the soil outside the loaded area remains relatively uninvolved, with minimal movement on both sides of the foundation (Siragy, 2019). The deformation process of the foundation entails compression of the soil directly beneath it and vertical shearing of the soil around the perimeter of the foundation.

Figure 8: Failure mode for existing footing model: (a) mod factor = 2.0; (b) mod factor = 2.5)

a **b**

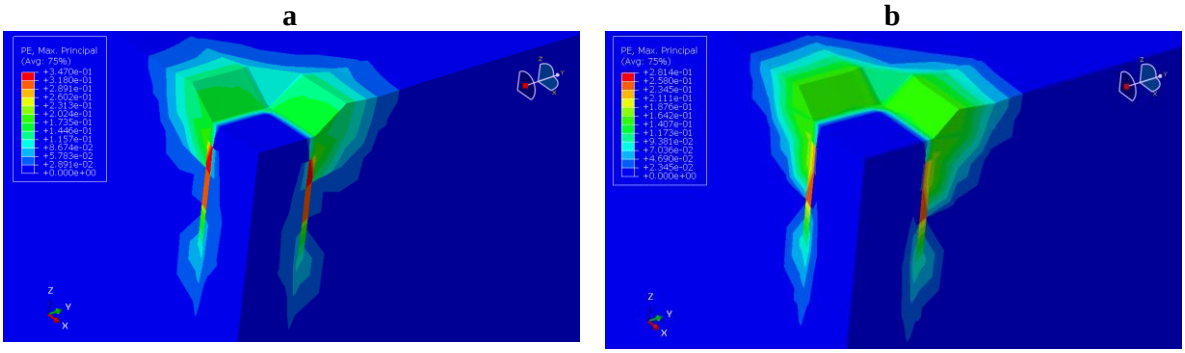

Article DOI: https://doi.org/10.37284/eaje.7.1.1991

Figure 9 is similar to the figures in liquefiable soil shown earlier. The (q)-settlement curve, as depicted in Figure 9, lacks a dramatic break, and the bearing capacity is often defined as the first measure of nonlinearity in this curve ($q_{u,o}$). Beyond the ultimate failure point ($q_{u,o}$), the (load/unit area)-settlement curve steepens, exhibiting a practically linear trend. Punching shear failure in the field proceeds as illustrated in the accompanying figure. This mode of failure can have significant implications for the stability and integrity of structures, particularly those with mat and other shallow foundations or subjected to uneven loading conditions.

Figure 9: Features of punching shear failure

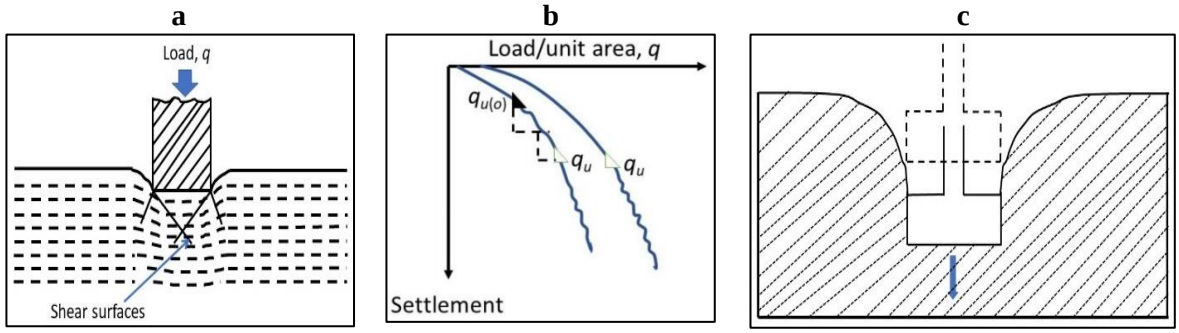

CONCLUSIONS

In order to construct a modified mat foundation that can support loads within the range seen for NLS, the study evaluated the performance of existing mat foundations in liquefiable soil and non-liquefiable soil. The existing mat foundation in liquefied sand could not provide the bearing capability of the same mat foundation in non-liquefied sand, according to preliminary simulations. Then customized design modifications and numerical simulations for liquefied soil conditions are performed. The results show that increasing bearing capacity may be achieved at a reasonable cost by using a modification factor ranging from 2.4 to 2.6, but of course, the specific value of the modification factor depends on the initial size of the foundation.

Furthermore, the identification of punching shear failure as a primary failure mode for modified mat footings emphasizes the necessity of considering such failure mechanisms in design considerations for mats and other shallow foundations.

The findings highlight the effectiveness of tailored design solutions in addressing the challenges posed by soil liquefaction conditions, and these findings can be used in foundation design to improve structural safety and integrity.

REFERENCE

Bahloul, M. M., Bahloul, M., Elshanwany, M. D., & Azzam, W. R. (2004). Strengthening of loaded footing-soil system by vertical extensible reinforcement. *5th International Conference on: Ground Improvement Technique*.

Coduto, D. P. (2015). *Foundation design: principles and practices*. Pearson.

Fan, Q., Feng, X., Weng, W., Fan, Y., & Jiang, Q. (2017). Unloading performances and stabilizing practices for columnar jointed basalt: A case study of Baihetan hydropower station. *Journal of Rock Mechanics and Geotechnical Engineering*, *9*(6), 1041–1053. https://doi.org/10.1016/j.jrmge.2017.07.003

Helwany, S. (2007). *Applied soil mechanics with ABAQUS applications*. John Wiley & Sons.

Jelušič, P., & Žlender, B. (2018). Optimal Design of Reinforced Pad Foundation and Strip Foundation. *International Journal of Geomechanics*, *18*(9), 1–11. https://doi.org/10.1061/(asce)gm.1943-5622.0001258

Kang, F., & Jie, P. (2017). Detailed explanation of ABAQUS geotechnical engineering examples. *Posts & Telecom Press: Beijing, China*.

Article DOI: https://doi.org/10.37284/eaje.7.1.1991

McGann, C. R., Arduino, P., & Mackenzie-Helnwein, P. (2012). *Development of simplified analysis procedure for piles in laterally spreading layered soils*.

Rostami, R., Hytiris, N., Bhattacharya, S., & Giblin, M. (2017). Seismic analysis of pile in liquefiable soil and plastic hinge. *Geotechnical Research*, *4*(4), 203–213. https://doi.org/10.1680/jgere.17.00009

Sarkar, R., Bhattacharya, S., & Maheshwari, B. K. (2014). Seismic requalification of pile foundations in liquefiable soils. *Indian Geotechnical Journal*, *44*, 183–195.

Siragy, M. (2019). Improving the ultimate capacity of loaded strip footing using additional contact area under excessive loads. *Life Sci J*, *16*(12), 147–153.

Terzaghi, K. (1943). *Theoretical soil mechanics*.

Terzaghi, K., Peck, R. B., & Mesri, G. (1996). *Soil mechanics in engineering practice*. John wiley & sons.

Zhang, J., Wang, T., Xiao, S., & Gao, L. (2021). Chinese code methods for liquefaction potential assessment based on standard penetration test: An extension. *Soil Dynamics and Earthquake Engineering*, *144*(February), 106697. https://doi.org/10.1016/j.soildyn.2021.106697

Zienkiewicz, O. C., Taylor, R. L., & Zhu, J. Z. (2005). *The finite element method: its basis and fundamentals*. Elsevier.

